Biochemical and Biophysical Research Communications 453 (2014) 662–667

Contents lists available at ScienceDirect

Biochemical and Biophysical Research Communications

journal homepage: www.elsevier.com/locate/ybbrc

Crystal structure of product-bound complex of UDP-*N*-acetyl-D-mannosamine dehydrogenase from *Pyrococcus horikoshii* OT3

K.J. Pampa [a,*], N.K. Lokanath [b], T.U. Girish [c], N. Kunishima [d], V.R. Rai [a]

[a] Department of Studies in Microbiology, University of Mysore, Mysore 570 006, India
[b] Department of Studies in Physics, University of Mysore, Mysore 570 006, India
[c] Department of General Surgery, JSS Medical College and Hospital, JSS University, Mysore 570 015, India
[d] Advanced Protein Crystallography Research Group, RIKEN SPring-8 Center, Harima Institute, Hyogo 679-5148, Japan

ARTICLE INFO

Article history:
Received 26 September 2014
Available online 8 October 2014

Keywords:
UDP-D-ManNAcADH
UDP-D-ManNAcA
Oligomerization domain
Thermostability

ABSTRACT

UDP-*N*-acetyl-D-mannosamine dehydrogenase (UDP-D-ManNAcDH) belongs to UDP-glucose/GDP-mannose dehydrogenase family and catalyzes Uridine-diphospho-*N*-acetyl-D-mannosamine (UDP-D-ManNAc) to Uridine-diphospho-*N*-acetyl-D-mannosaminuronic acid (UDP-D-ManNAcA) through twofold oxidation of NAD^+. In order to reveal the structural features of the *Pyrococcus horikoshii* UDP-D-ManNAcADH, we have determined the crystal structure of the product-bound enzyme by X-ray diffraction to resolution of 1.55 Å. The protomer folds into three distinct domains; nucleotide binding domain (NBD), substrate binding domain (SBD) and oligomerization domain (OD, involved in the dimerization). The clear electron density of the UDP-D-ManNAcA is observed and the residues binding are identified for the first time. Crystal structures reveal a tight dimeric polymer chains with product-bound in all the structures. The catalytic residues Cys258 and Lys204 are conserved. The Cys258 acts as catalytic nucleophile and Lys204 as acid/base catalyst. The product is directly interacts with residues Arg211, Thr249, Arg244, Gly255, Arg289, Lys319 and Arg398. In addition, the structural parameters responsible for thermostability and oligomerization of the three dimensional structure are analyzed.

1. Introduction

UDP-*N*-acetyl-D-mannosamine dehydrogenase (UDP-D-ManNAcDH, EC 1.1.1.336) catalyzes the Uridine-diphospho-*N*-acetyl-D-mannosamine (UDP-D-ManNAc) to Uridine-diphospho-*N*-acetyl-D-mannosaminuronic acid (UDP-D-ManNAcA) using NAD^+ as cofactor. The sequence and structural similarities revealed that UDP-D-ManNAcDH belongs to UDP-glucose/GDP-mannose dehydrogenase family. And these enzymes catalyze a net four-electron oxidation and serve as both (aldehyde and alcohol) dehydrogenase [1]. UDP-D-ManNAc and UDP-D-ManNAcA are ubiquitous and essential intracellular metabolite in cellular processes. And, they play the role of precursors for proteoglycans and glycoproteins as well as the cell wall components of the bacteria. The UDP-D-ManNAc acts as a precursor for the linkage unit synthesis in the *Staphylococcus aureus* H, *Micrococcus vaians* and *Bacillus subtilis* W23 [2]. UDP-D-ManNAcA is used as substrate for glycotransferases [3]. Oligosaccharide chains (*O*- and *N*-glycans) and glycolipids are established with major contribution from *N*-Acetyl-*O*-mannosamine [4]. UDP-D-ManNAcA is synthesized from UDP-*N*-acetyl-D-glucosamine (UDP-D-GlcNAc), by means of two-step pathway. In the first step, UDP-*N*-acetylglucosamine 2-epimerase catalyzes the C-2 epimerization of UDP-D-GlcNAc to form UDP-D-ManNAc, and in the second step, UDPManNAcDH catalyzes the C-6 dehydrogenation of UDP-D-ManNAc to form UDP-D-ManNAcA [5]. The protein *Cap50* from *S. aureus* (*Sa*) showed sequence homology to *Ph*UDPManNAcADH, from *Escherichia coli* which acts in the biosynthesis of the enterobacterial common antigen [6]. *Cap50* catalyzes the oxidation of UDP-D-ManNAc to UDP-D-ManNAcA and recently the structure of *Sa*UDPManNAcDH is reported [6]. The structural relevance from available crystal structure display high similarity in α/β fold pattern in homodimeric and with typical Rossmann like folds [7]. The multiple sequence alignment revealed the nucleotide binding motif *G-X-G-X-X-G* (Supplemental Fig. S1) of N-terminal α/β domain to be common in all the enzymes [8,9]. We have reported the purification and the crystallization of UDP-D-ManNAcADH from *Pyrococcus horikoshii* [10].

Further, the investigation is carried out to understand the biosynthesis pathway of UDP-D-ManNAcA and catalytic mechanism.

* Corresponding author.
E-mail address: sagarikakj@gmail.com (K.J. Pampa).

http://dx.doi.org/10.1016/j.bbrc.2014.10.010
0006-291X/

Herein, we report the structure of *Ph*UDP-D-ManNAcADH complex (enzyme with product) with UDP-*N*-acetyl-D-mannosaminuronic acid (UDP-D-ManMAcA) using X-ray diffraction to a resolution of 1.55 Å. To our knowledge, this is the first detailed 3-D structural characterization of *Ph*UDP-D-ManNAcADH complex with UDP-D-ManMAcA. The monomeric structure consists of three distinct domains; N-terminal domain (nucleotide binding domain), central helical domain (involved in dimerization) and C-terminal domain (substrate binding domain). This product-complex structure will provide a path in recognizing the substrate binding residues which may provide the structural basis for enzymatic catalysis. In addition, oligomerization and thermostability of the enzyme are analyzed.

2. Materials and methods

2.1. Protein and purification

The *Ph*UDP-D-ManNAcADH was purified and crystallized as described [10]. For the preparation of SeMet-substituted protein, the BL21 (DE3)Star (Invitrogen) cells were grown in M9 medium until they reached an absorbance at 600 nm (A600) of 0.4. At this point, 100 mg of L-lysine, 100 mg of L-phenylalanine, 100 mg of L-threonine, 50 mg of L-isoleucine, 50 mg of L-leucine and 60 mg of SeMet were added to 1 l of culture and the cells were grown at 37 °C for a further 1 h, before inducing the expression with 1 mM IPTG overnight at 25 °C. The protein was purified using SuperQ Toyopearl 650, ResourceQ, Hydroxylapatite and Superdex 200 columns. The purified protein was concentrated to 15.8 mg/ml for crystallization studies.

2.2. Crystallization and data collection

The SeMet-substituted *Ph*UDP-D-ManNAcADH was crystallized using microbatch sitting method under reservoir solution condition 10% (*w/v*) PEG 8000, 8% (*v/v*) ethylene glycol and 0.1 M HEPES pH 7.5. Data sets were collected at the synchrotron beam line BL26B1 at SPring-8, Japan, under cryogenic conditions. Crystals were flash-frozen with liquid nitrogen at 100 K in their respective mother liquor or soaking solution containing 24% (v/v) glycerol as cryoprotectant. The RIGAKU CCD detector was used for data collection. The data were processed and scaled using HKL 2000 suite [11]. The datasets were completed by including all possible *hkl* and R_{free} columns using UNIQUE of CCP4 suite [12]. The data collection parameters and processing statistics are given in Supplementary Table 1.

2.3. Structure determination and refinement

The structure of *Ph*UDP-ManNAcADH was solved by multi-wavelength anomalous dispersion phasing method [13] using the automatic structure determination software SOLVE [14]. Refinement was carried out using CNS [15]. The model was further improved using the graphics program COOT [16] through its real space fitting and interactive manual building. A blob of positive density was observed in *Fo–Fc* map at 3.0 σ level at the active site of the *Ph*UDP-ManNAcADH structure that could be interpreted as a UDP-D-ManMAcA molecule. Stereochemical quality of the coordinates was checked with the program PROCHECK [17]. The final atomic coordinates of *Ph*UDP-ManNAcADH are deposited in the RCSB Protein Data Bank (http://www.rcsb.org/pdb) with the accession codes 4R16. The refinement statistics are given in Supplementary Table 1.

2.4. Model analysis

DALI [18] (http://ekhinda.biocenter.helsinki.fi/daliserver/start) server was utilized for structural similarity search against all known structures deposited in the protein data bank. All figures were prepared using PyMol (http://www.pymol.org). Surface areas for dimer and hydrogen bonds were calculated using PISA [19]. The ionic bridges were calculated using ESBRI [20]. Aromatic-aromatic interactions and cation-pi interactions were calculated using PIC [21]. Multiple sequence alignment is performed using CLUSTALW [22], and the figure was generated using ESPript [23]. The structures were superposed using LSQKAB program, integrated in CCP4i [12].

3. Results and discussions

3.1. Overall structure

In the monomeric structure of *Ph*UDP-ManNAcADH (Fig. 1A), a residue range of 1–196 assembled to N-terminal domain (NBD – nucleotide binding domain) consists of six-stranded parallel β-sheets (β1–β6). These sheets are surrounded with five helices (α1–α5) and followed by two anti-parallel β-sheets (β7–β8) with two helices (α6–α7). The residues from 303–420 configures to C-terminal domain (SBD – substrate binding domain) and mimics the first five β-sheets of the NBD and it is packed with helices (α12–α13). These two domains are connected by a central helical domain (OD – oligomerization domain; 197–302: Fig. 1B) composed of helices α8, α9, α10 and α11. The UDP-D-ManMAcA molecule is bound in cleft between the three domains, NBD, SBD and OD (Fig. 1C).

3.2. Product binding site

During crystallization, no product was added to the *Ph*UDP-D-ManNAcADH solution (Table 1). However, the crystal structure reveals the presence of product-bound, UDP-D-ManMAcA. For the first time, a clear electron density for inbound UDP-D-ManMAcA molecule was observed in the active site of the *Ph*UDP-D-ManNAcADH (Fig. 2A). The C-terminal α/β domain and central helical domain participates in UDP-D-ManNAcA binding pocket (Fig. 2B). The C-terminal domain is primarily responsible for binding the UDP moiety of the product in a deep pocket adjacent to the middle of the central α helix. Residues Arg211, Thr249, Arg244, Gly255, Arg289, Lys319 and Arg398 were directly hydrogen bonds with the UDP-D-ManNAcA (Fig. 2B and Table 2). The residues, Lys204 and Asn208 make the hydrogen bonds to the atom O6 of the product. The product atoms O3* and O7* forms the hydrogen bonds to Arg244, and atom N2* make hydrogen bond to the residue Asn208. The phosphate group moiety atoms O2A and O1A hydrogen bonds to Arg211, and O2A make polar contact with Lys319. The ribose moiety atoms (O3 and O2) make hydrogen bonds with Gly255 and Arg398, respectively. And Thr249 hydrogen bonds with N3 and O4 atoms of the product. Also, the residues Cys258, Thr119, Asp262, Tyr10, His257, Tyr318, Gly253, Leu259 and Thr249 make hydrogen bonds with the product through the water molecules (Supplemental Fig. S1). The only residue Tyr10 from consensus sequence interacts with the UDP-D-ManNAcA, through water molecule.

In addition we attempted to cocrystallize the enzyme with different concentration of cofactor (NAD). However, we could not obtain good diffracting cofactor complex crystals. In order to explain the stoichiometry of the purified enzyme, our crystal data shows strong affinity to the substrate, UDP-*N*-acetyl-D-mannosaminuronic acid. Though we did not include substrate during the crystallization of the enzyme, the presence of product in the crystal might have originated from the host organism *E. coli*, which is used for expression. Therefore purified enzyme is always bound with the substrate or product.

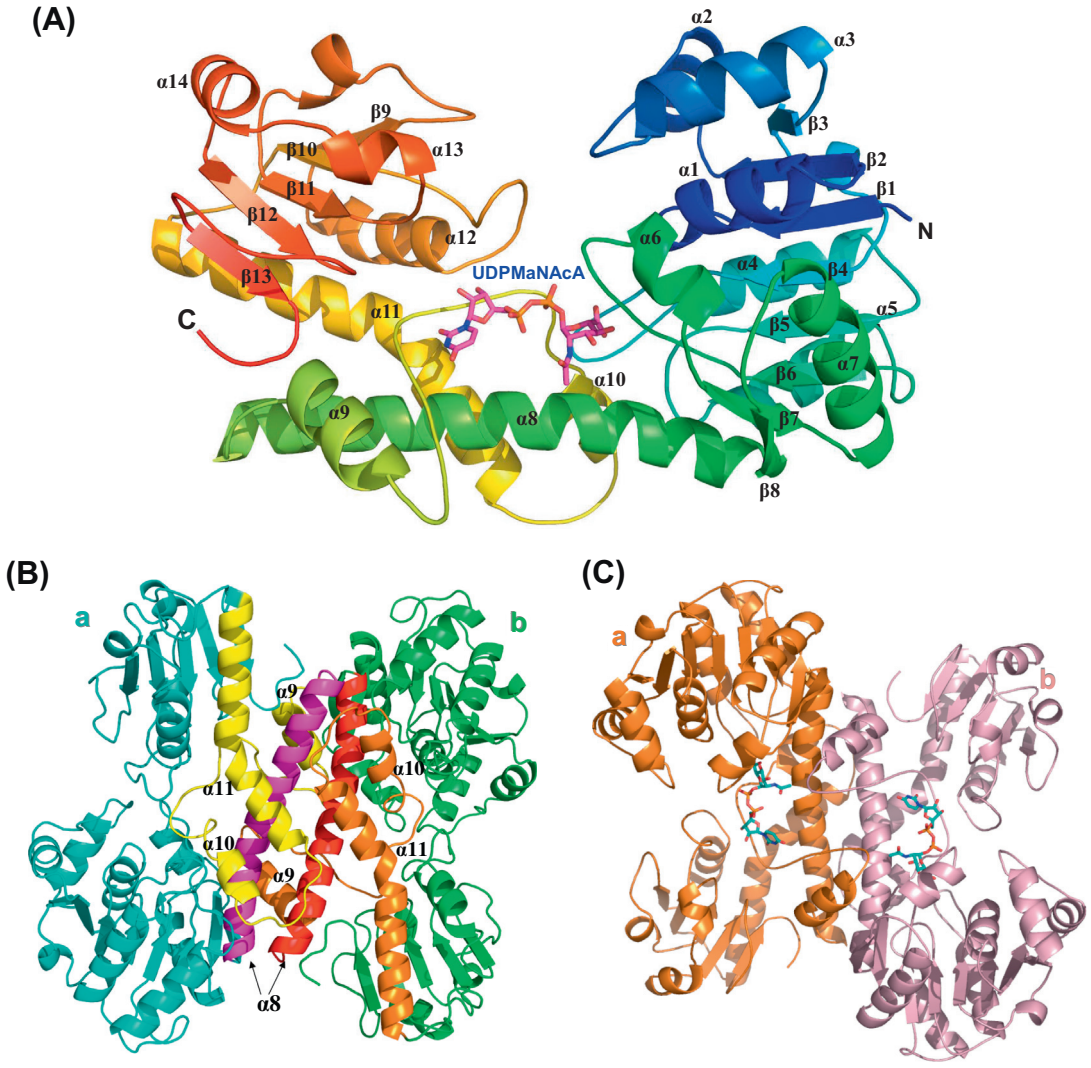

Fig. 1. Overall ribbon representation of *Ph*UDP-D-ManNAcADH. (A) The monomeric structure of *Ph*UDP-D-ManNAcADH, mainly composed of nucleotide binding domain (residues 1–196), substrate binding domain (residues 303–420). The UDP-D-ManNAcA molecule is shown as ball-and-stick model (magenta). N-terminal and C-terminal are marked correspondingly. (B) Oligomerisation domain helices are colored red, yellow, magenta and orange. The green and cyan color represents the subunits a and b. (C) Dimeric structure of *Ph*UDP-D-ManNAcADH. UDP-D-ManNAcA molecule is shown as ball-and-stick model. (For interpretation of the references to color in this figure legend, the reader is referred to the web version of this article.)

3.3. Oligomerization and thermostability

Crystallogarphic analyses reveal that *Ph*UDP-D-ManNAcADH exists as an apparent dimer in the crystal with extensive interfaces. The observed dimers are consistent with the results of dynamic light-scattering studies showing the dimeric state of UDP-ManNAcADH in solution [10]. The *Ph*UDP-D-ManNAcADH is assembled *via* high affinity interactions between two protomer to form homodimers (Fig. 1B). The monomers aggregate to dimeric form with major interactions from oligomerization domain residues. The helices of oligomerization domain α8, α9 and α11 (Fig. 1C) of subunit (A) interacts with the same helices of other protomer (B). The observed oligomeric state might be important for the catalytic function through forming the active site involving the adjacent subunit, which seems to be conserved in the UDP-glucose dehydrogenases. There are twenty-six hydrogen bonds between the subunits, three pair of ion pairs (I–P's) [Glu161 (A/B) – Arg244 (B/A) and Glu207 (A) – His242 (B)] and two pair of cation – pi (C–P's) interactions [Phe274 (A/B) – Arg286 (B/A)]. The interface between the dimer shows a buried surface area of 2750 Å^2, which corresponds 14.5% of the total protomer surface area. This interface is mediated by the helical portion of the C-terminal domain majority of the solvent accessible surface area, followed by the central α-helix, and the N-terminal domain. The interacting surfaces at interface are essentially hydrophobic. These interactions present at the dimer interface can provide *Ph*UDP-D-ManNAcADH to perform the catalysis at higher temperature [24]. The structural features such as aromatic–aromatic (A–A), C–P and I–P interactions contribute to the protein stability at high temperature. Here, we evaluated the mentioned parameters with *Ph*UDP-D-ManNAcADH (thermophile) and *Sa*UDP-D-ManNAcDH (mesophile) (Supplemental Table 1(a–c)). The *Ph*UDP-D-ManNAcDH has twenty-four I–P's, three A–A's and six C–P's, while mesophile has twenty I–P's, seven A–A's and four C–P's. The thermophile has more number of I–P's and C–P's, whereas mesophilic has more A–A's.

3.4. Active site residues

There is no structural report on the complete enzymatic reaction of UDP-D-ManNAcADH with UDP-D-ManMAcA. However, crystal structure of UDP-ManNAcDH from *S. aureus* (Cap50) was

Table 1
Crystal data, data collection and refinement statistics of *Ph*UDP-D-ManNAcADH.

Data statistics	
Space group	P $\bar{1}$
Unit-cell parameters (Å, °)	54.03, 74.65, 73.56, 66.2, 70.4, 75.2
V_M (Å^3 Da^{-1})	2.3
Content of the asymmetric unit	2
Resolution (Å)	50.0–155 (1.61–1.55)
Reflections (measured/unique)	135,913/135,911
R_{merge} (%)	5.6
Completeness (%)	95.6
$<I/\sigma(I)>$	9.6
Redundancy	2.9
Refinement statistics	
Resolution (Å)	40.0–155
R_{cryst} (%)	22.4
R_{free} (%)	25.0
rms bond lengths (Å)	0.004
rms bond angles (°)	1.28
Ramachandran plot (%)	
Most favored	90.9
Additional	8.6
Generous	0.6

Table 2
Hydrogen bonding distance between UDP-D-ManNAcA and the residues.

UDP-D-ManNacA atom	Interacting residue	Distances in Å
O4	Thr249 (N)	2.90
	Thr249(O)	2.90
O2′	Arg398(NH1)	2.85
O3′	Gly255(N)	2.85
O1A	Lys319(NZ)	2.96
	Arg211(NH2)	3.13
O2A	Arg211(NE)	2.70
N2*	Asn208(OD1)	2.90
O7*	Arg244 (NE)	2.75
O3*	Arg244(NH2)	2.91
O6A	Asn208(ND2)	2.65
O6A	Lys204(NZ)	2.78

reported [7]. The residues involved in the catalytic mechanism are Cys258, Lys204, Asp262, Thr119, Asn208 and Glu151 (Fig. 3) conserved throughout the family (Supplemental Fig. S1). These active site residues are also conserved in *Cap50* and other dehydrogenases of the same family [6]. It is evident from the structure,

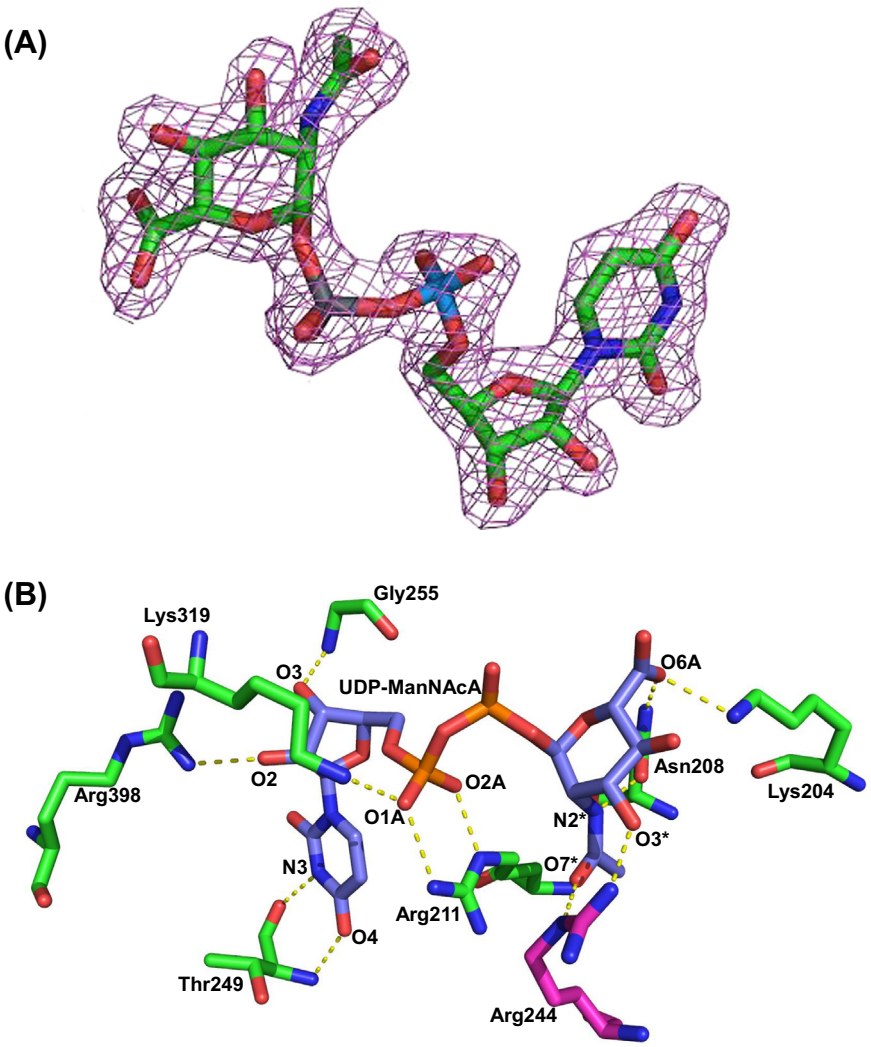

Fig. 2. Product-bound in the active site. (A) UDPManNAcA (green colored ball-and-stick model) shown within electron density map contoured at 1.5 σ. (B) Product binding residues; UDP-D-ManNAcA is represented by purple ball-and-stick model. The interacting residues are represented by green colored ball-and-stick model (same monomer) and magenta colored ball-and-stick model (from other protomer). Yellow dotted lines indicate hydrogen bonding. (For interpretation of the references to color in this figure legend, the reader is referred to the web version of this article.)

Cys258 is involved in the thioester formation and Lys204 acts as acid/base catalyst involved in hydride transfer. And, therefore, the residue Cys258 acting as catalytic nucleophilic and Lys204 acts as acid/base catalyst (Fig. 3a and b). The base is responsible for deprotonating the alcohol product during the first oxidation and contributing to stabilization of the tetrahedral intermediate during the second oxidation. Residues Asp262, Thr119, Asn208 and Glu151 provides platform for water molecules to be involved in the catalysis.

3.5. Structural comparisons

The 3-D structural similarity search is performed using DALI server for *Ph*UDP-D-ManNAcADH coordinates with the available structures of the Protein Data Bank. The closest structural homologue was found to be *Sa*UDP-ManNAcDH (*Cap50*, PDB code: 3ojl), with *Z* score of 46.3, sequence similarity of 42% and the r.m.s.d. value is 2.9 Å [7]. The structure of *Sa*UDP-ManNAcDH is superposed with the structure of *Ph*UDP-D-ManNAcADH (Fig. 4), revealed a conserved secondary structures with little deviations. The observed deviations may be due to the product (UDP-D-ManNAcA) binding. The other similar enzymes are listed in Table 3.

In conclusion, we have determined the high resolution crystal structure of *Ph*UDP-D-ManNAcADH with the product UDP-D-ManNAcA. This work may provide structural platform for elucidating enzymatic catalysis. The evidence presented here successfully identified the active site and provided the molecular basis for understanding the catalytic mechanism of *Ph*UDP-D-ManNAcADH. The structural features responsible for thermostability are evaluated. Further biochemical studies and substrate-cofactor/product-cofactor complex with the enzyme will most likely underline the importance of this enzyme.

Acknowledgments

The authors would like thank the IOE single crystal X-ray diffraction facility, University of Mysore, Mysore. Authors would like to thank the beamline staff for assistance during data collection at beamline BL26B1 of SPring-8, Japan.

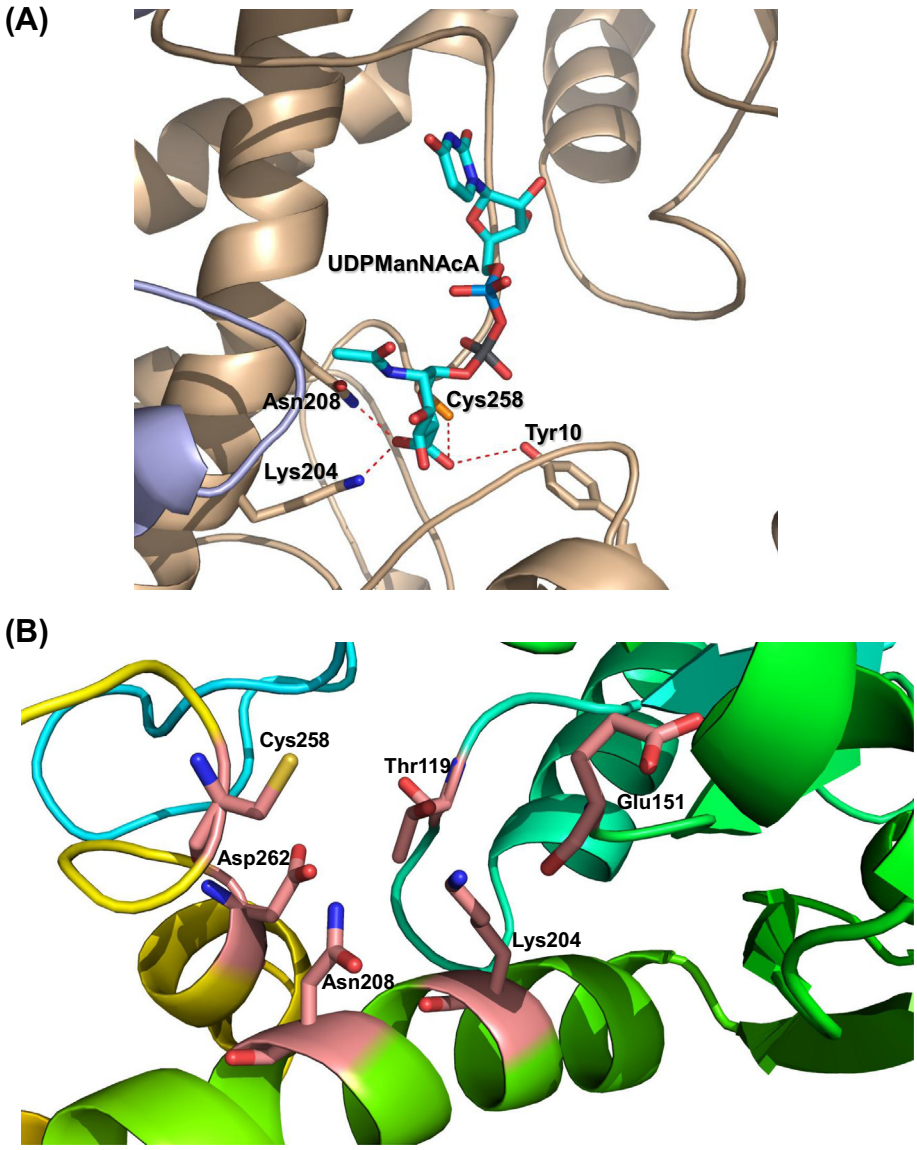

Fig. 3. Active site residues. (A) UDP-D-ManNAcA and important residues are depicted as ball-and-stick models and labeled. Secondary structure from other subunit is shown in light blue color. Important hydrogen bonds are indicated by broken lines (red). (B) The orange colored ball-and-stick model represents the residues involved in catalysis. The residues are Thr119, Glu151, Lys204, Asn208, Cys258 and Asp262. (For interpretation of the references to color in this figure legend, the reader is referred to the web version of this article.)

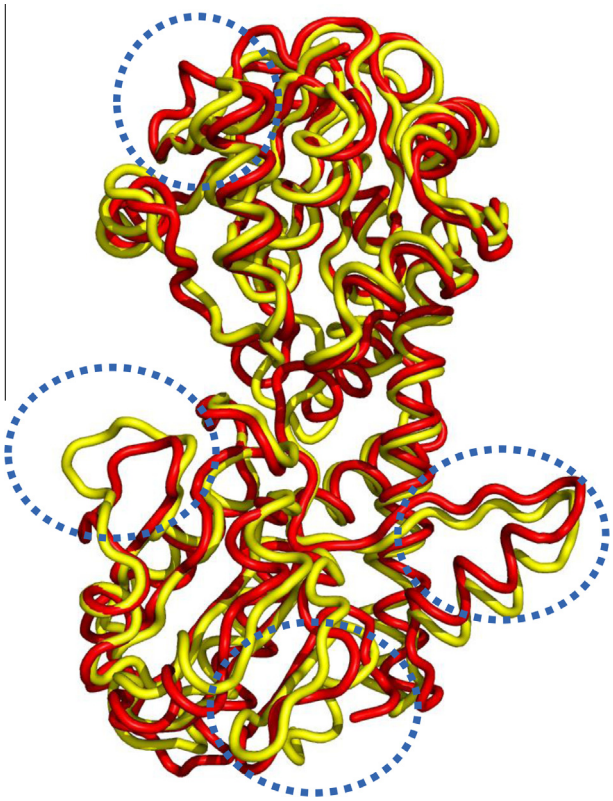

Fig. 4. Structural superposition of *Ph*UDP-D-ManNAcADH protomer (yellow) with the *Sa*UDP-ManNAcDH (red). Dotted circles (blue color) represent the observed differences between these two structures. (For interpretation of the references to color in this figure legend, the reader is referred to the web version of this article.)

Table 3
r.m.s. deviation with *Ph*UDP-D-ManNAcADH (4R16).

Enzyme	Z-score	Sequence similarity (%)	r.m.s.d (Å)	Number of aligned C_α atoms
3ojl	46.3	42	2.9	409
3gg2	45.2	28	1.7	399
3vtf	44.8	31	1.7	385
4a7p	44.8	27	1.8	398

r.m.s.d (root mean square deviation).

Appendix A. Supplementary data

Supplementary data associated with this article can be found, in the online version, at http://dx.doi.org/10.1016/j.bbrc.2014.10.010.

References

[1] X. Ge, L.C. Penny, I. Van de Rijin, M.E. Tanner, Active site residues and mechanism of UDP-glucose dehydrogenase, Eur. J. Biochem. 271 (2004) 14–22.
[2] C.R. Harrington, J. Baddiley, Biosynthesis of wall tiechoic acids in *Staphylococcus aureus* H, *Micrococcus varians* and *Bacillus subtilis* W23, Eur. J. Biochem. 153 (1985) 639–645.
[3] S.C. Namboori, D.E. Graham, Enzymatic analysis of uridine diphosphate *N*-acetyl-D-glucosamine, J. Bacteriol. 190 (2008) 2987–2996.
[4] H. Schachter, The joys of HexNAc. The synthesis and function of *N*-and *O*-glycan branches, Glycoconj. J. 17 (2000) 465–483.
[5] M.F. Reid, C.A. Fewson, Molecular characterization of microbial alcohol dehydrogenases, Crit. Rev. Microbiol. 20 (1994) 13–56.
[6] U. Meier-dieter, R. Starman, K. Barr, H. Mayer, P.D. Rick, Biosynthesis of enterobacterial common antigen in *Escherichia coli*. Biochemical characterization of Tn10 insertion mutants defective in enterobacterial common antigen synthesis, J. Biol. Chem. 265 (1990) 13490–13497.
[7] J. Gruszczyk, A. Fleurie, V. Olivares-Illana, E. Bechet, I. Zanella-Cleon, S. Morera, P. Meyer, G. Pompidor, R. Khan, C. Grangeasse, Structure analysis of the *Staphylococcus aureus* UDP-*N*-acetyl-mannosamine dehydrogenase cap50 involved in capsular polysaccharide biosynthesis, J. Biol. Chem. 286 (2011) 17112–17121.
[8] M.G. Rossmann, D. Moras, K.W. Olsen, Chemical and biological evolution of nucleotide-binding protein, Nature 250 (1974) 194–199.
[9] R.K. Wierenga, M.C.H. De Maeyer, W.G.J. Hol, Interaction of pyrophosphatase moieties with alpha-helixes in dinucleotide binding proteins, Biochemistry 24 (1985) 1346–1357.
[10] N.K. Lokanath, K.J. Pampa, Toshimi Kamiya, Naoki Kunishima, Purification, crystallization and preliminary X-ray diffraction studies of a putative UDP-*N*-acetyl-D-mannosamine dehydrogenase from *Pyrococcus horikoshii* OT3, Acta Crystallogr. F Struct. Biol. Commun. 63 (2007) 412–414.
[11] Z. Otwinowski, W. Minor, Processing of X-ray diffraction data collected in oscillation mode, Methods Enzymol. 276 (1997) 307–326.
[12] Collaborative Computational Project, Number 4, the CCP4 suite: programs for protein crystallography, Acta Crystallogr. D Biol. Crystallogr. 50 (1994) 760–763.
[13] W.A. Hendrickson, J.R. Horton, D.M. LeMaster, Selenomethionyl proteins produced for analysis by multiwavelength anomalous diffraction (MAD): a vehicle for direct determination of three-dimensional structure, EMBO 9 (1990) 1665–1672.
[14] T.C. Terwilliger, J. Berendzen, Automated MAD and MIR structure solution, Crystallogr. D Biol. Crystallogr. 55 (1999) 849–861.
[15] P. Emsley, K. Cowtan, Coot: model-building tools for molecular graphics, Acta Crystallogr. D Biol. Crystallogr. 60 (2004) 2126–2132.
[16] A.T. Brunger, P.D. Adams, G.M. Clore, W.L. DeLano, P. Gross, R.W. Grosse-Kunstleve, J.S. Jiang, J. Kuszewski, M. Nilges, N.S. Pannu, L.M. Rice, T. Simson, G.L. Warren, Crystallography & NMR System: a new software suite for macromolecular structure determination, Acta Crystallogr. D Biol. Crystallogr. 54 (1998) 905–921.
[17] R.A. Laskowski, M.W. MacArthur, D.S. Moss, J.M. Thornton, PROCHECK: a program to check the stereochemical quality of protein structures, J. Appl. Cryst. 26 (1993) 283–291.
[18] L. Holm, C. Sander, Dali: a network tool for protein structure comparison, Trends Biochem. Sci. 20 (1995) 478–480.
[19] E. Krissinel, K. Henrick, Detection of protein assemblies in crystals, in: Berhold Mrea (Ed.), Computational Life Sciences, Springer, Berlin, Heidelberg, 2005, pp. 163–174.
[20] (a) S. Kumar, R. Nussinov, Salt bridge stability in monomeric proteins, J. Mol. Biol. 293 (1999) 1241–1255;
(b) S. Kumar, C.J. Tsai, B. Ma, R. Nussinov, Contribution of salt bridges toward protein thermostability, J. Biomol. Struct. Dyn. 1 (2000) 79–85;
(c) S. Kumar, R. Nussinov, Relationship between ion pair geometries and electrostatic strengths in proteins, Biophys. J. 83 (2002) 15595–15612;
(d) J.N. Sarakatsannis, Y. Duan, Statistical characterization of salt bridges in proteins, Proteins 60 (2005) 732–739.
[21] K.G. Tina, R. Bhadra, R. Srinivasan, PIC: protein interactions calculator, Nucleic Acids Res. 35 (2007) 473–476.
[22] J.D. Thompson, D.G. Higgins, T.J. Gibson, CLUSTAL W: improving the sensitivity of progressive multiple sequence alignment through sequence weighting, position-specific gap penalties and weight matrix choice, Nucleic Acids Res. 22 (1994) 4673–4680.
[23] P. Gouet, E. Courcelle, D.I. Stuart, ESPript: analysis of multiple sequence alignments in PostScript, Bioinformatics 15 (1999) 305–308.
[24] N.K. Lokanath, I. Shiromizu, N. Ohshima, Y. Nodakke, M. Sugahara, S. Kuramitsu, M. Miyano, N. Kunishima, Structure of aldolase from *Thermus thermophilus* HB8 showing the contribution of oligomeric state to thermostability, Acta Crystallogr. D Biol. Crystallogr. 60 (2004) 1816–1823.